Recent Results on B Physics from CLEO

Alan Weinstein

California Institute of Technology
Pasadena, CA 91125 USA
E-mail: ajw@caltech.edu

For the CLEO Collaboration

Abstract

I review selected recent (summer 1997) results from the CLEO experiment on B meson decays. The focus is on three main topics: exclusive hadronic decays from the $b \to c\bar{u}d$ process, rare decays from the $b \to u\bar{u}d$, $b \to sg$, and $b \to s\ell^+\ell^-$ processes, and exclusive semileptonic decays from the $b \to c\ell\nu$ and $b \to u\ell\nu$ processes.

Talk presented at *Beauty '97, UCLA, October 13, 1997*

1 Introduction

The CLEO experiment pursues a broad program in the physics of B meson decays, charmed meson and baryon spectroscopy and decay, τ lepton decay, Υ spectroscopy, two photon physics, and QCD studies. In this talk, I will review selected results from CLEO in B meson decay physics from summer, 1997. In particular, I will focus on three main topics. (a) A study of exclusive hadronic decays from $b \to c\bar{u}d$ transitions[1], including extractions of model parameters, tests of factorization, and a search for color suppressed decays. (b) Results on several classes of rare (non-$b \to c$) B meson decays: hadronic decays to two pseudoscalars, pseudoscalar and vector, or two vector mesons, which arise from $b \to u\bar{u}d$ and/or $b \to sg$ processes; and a search for the electroweak penguin decay $b \to s\ell^+\ell^-$. (c) Results on the semileptonic B decays $B \to D\ell\nu$, $B \to D^{**}\ell\nu$, and $B \to \rho\ell\nu$, $\omega\ell\nu$.

1.1 The CLEO Experiment and Data Sample

The CLEO II experiment operates at the Cornell e^+e^- Storage Ring (CESR), running at or near the peak of the $\Upsilon(4S)$ ($e^+e^- \to \Upsilon(4S) \to B\bar{B}$). On resonance, the $B\bar{B}$ cross section is 1.07 nb, on top of a "$udsc$" continuum cross section of 3.2 nb. CLEO typically runs 2/3 of the time on-resonance, 1/3 off (below $B\overline{B}$ threshold, in order to study the properties of the continuum events). CLEO II collected data from 1989 through 1995, accumulating an integrated luminosity of $\mathcal{L} = 5$ fb^{-1}, corresponding to over 3 million $B\overline{B}$ events on tape. The CLEO II.V detector added a silicon vertex detector in 1995, and has accumulated $\mathcal{L} = 4.1$ fb^{-1} to date. The CLEO III detector is in preparation for first data taking in 1999, along with an upgraded CESR collider with 4 times the current peak luminosity. CLEO III will feature an entirely new inner detector: new silicon vertex detector, drift chamber, fast RICH for K/π separation at momenta up to 2.6 GeV, a new data acquisition system, and new software infrastructure.

The results presented in this talk are based on the 3.3 million $B\overline{B}$ events collected by the CLEO II detector from 1990 through 1995. Most of these results use full reconstruction of one B meson decay. We identify pions and kaons using dE/dx in the tracking chambers and time-of-flight measurement from the TOF scintillator system. We identify electrons using dE/dx and

[1]Throughout this paper, references to decay chains and final states also imply their charge conjugates.

the ratio E/p of shower energy in the calorimeter to momentum measured in the tracking system. We identify muons using counters placed behind absorbers of thickness 3, 5, and 7 hadronic interaction lengths (minimum). We exploit the fact that at the $\Upsilon(4S)$, each B has the beam energy and small momentum ($\sim$ 300 MeV/c), by requiring the excess energy of the candidate B meson, $\Delta E = E_{candidate} - E_{beam}$, to be small, and the "beam-constrained mass" $M_b = \sqrt{E_{beam}^2 - P_{candidate}^2}$ to be near the known B mass $M_B = 5.279$ GeV/c^2.

To suppress backgrounds, we require a spherical event shape characteristic of $B\overline{B}$ events, in contrast to the jetty energy flow characteristic of *udsc* continuum events. We suppress some forms of combinatoric background by exploiting the fact that the decay products of one B are uncorrelated in angle with the decay products of other B in the event. In decays involving vector mesons, further background suppression can be obtained by cutting on the helicity angle(s) of the daughter meson decays. For rare B decays, much more stringent background suppression is required, as discussed later in this paper.

2 $B \to D^{(*)}(n\pi)$

CLEO has reconstructed, and measured the branching ratios for, a family of exclusive quasi- two-body hadronic decays of the form $D^{(*)}(n\pi)$ [1, 2]. The entire decay chain is reconstructed, using the following daughter decays:

- $D^0 \to K^-\pi^+$, $K^-\pi^+\pi^0$, $K^-\pi^+\pi^-\pi^+$; or $D^+ \to K^-\pi^+\pi^+$
- $D^{*+} \to D^0\pi^+$ or $D^{*0} \to D^0\pi^0$
- $\rho^+ \to \pi^+\pi^0$, $\rho^0 \to \pi^+\pi^-$, or $a_1 \to 3\pi$

The decays in which the $(n\pi)$ system has net charge non-zero are "color-allowed" and those of the form $B^0 \to D^{(*)0}(n\pi)^0$ are "color-suppressed" (see below). There are strong signals for all the color-allowed decays; the numbers of events, and derived branching fractions, are listed in Table 1. No significant signals are seen for any of the color-suppressed decay modes; upper limits are listed in Table 2.

There is no evidence for non-resonant $D^{(*)}(2\pi)$ (*i.e.*, not from $\rho \to 2\pi$) or non-resonant $D^{(*)}(3\pi)$ (*i.e.*, not from $a_1 \to 3\pi$) and upper limits are set on these non-resonant processes.

2.1 Interpretation within BSW model

In order to interpret these results, we need to work within a model that, at least qualitatively, describes these hadronic decays. A useful framework is that of the Bauer-Stech-Wirbel (BSW) model[3], which divides these quasi-two-body final states into three classes, parameterized with two parameters, a_1 and a_2. Class I is "external spectator" decays, in which the W^- in $b \to cW^-$ hadronizes independently from the recoil c quark plus spectator quark. Examples are $B^0 \to D^{(*)+}(n\pi)^-$ and $B^0 \to D^{(*)+}D_s^{(*)-}$. The decay rates are proportional to $|a_1|^2$ (with mode-dependent pre-factors that depend only on $G_F|V_{cb}|$, phase space, and Clebsch-Gordon coefficients). Class II is "color-suppressed" decays, in which the quarks from the W^- must combine with the c quark plus spectator quark in order to hadronize. Examples are $B^0 \to D^{(*)0}(n\pi)^0$ and $B^{\pm,0} \to \psi K^{(*)\pm,0}$. The decay rates are proportional to $|a_2|^2$. Class III decays involve both types of diagrams. Examples are $B^- \to D^{(*)0}(n\pi)^-$ and $B^- \to D^{(*)0}K^-$. The decay rates are proportional to $|a_1 + xa_2|^2$, where x is a mode-dependent pre-factor. The parameters a_1 and a_2 are in principle calculable from the Wilson coefficients of perturbative QCD, but in practice are treated as parameters to be fitted for.

This model assumes factorization, so that the decay amplitude factorizes into the dot product of two currents. For the color-allowed decays,

$$\begin{aligned}
\Gamma &\propto \left|\left\langle D^{(*)}|J_\mu|B\right\rangle \left\langle (n\pi)^-|J_\mu|0\right\rangle\right|^2 \\
&\propto \left|FF(B \to D^{(*)})a_1 f_{n\pi}\right|^2
\end{aligned}$$

and similarly for color-suppressed and class III decays. In D decays, 2-body decays ($D \to K^{(*)}\pi^{(*)}$) dominate, and a_2/a_1 is *negative*, so charged D decays (class III) have negative interference. This is believed to be the origin of the large difference in lifetimes between the charged and neutral D mesons: $\tau(D^+) \simeq 2.5\tau(D^0)$. In B decays, 2-body decays are a small fraction of the total hadronic width, so any interference should have little effect on the total lifetime ratio. The current experimental ratio is $\tau(B^+)/\tau(B^0) = 1.06 \pm 0.04$.

Using the branching fractions presented above, and model predictions for the mode-dependent pre-factors, we can measure $|a_1|$ and the ratio a_2/a_1. The results, using the "BSW II"[3, 4] and CDDFGN[5] models, are given in Table 6.

The $\chi^2/\mathrm{dof} = 20.3/6$ with the CDDFGN model and $9.1/6$ for the BSW model; so the latter model gives a good fit to the data. The results depend on the ratio of B^+B^- to $B^0\bar{B}^0$ produced at the $\Upsilon(4S)$; this ratio is assumed to be 1 for the values quoted in Table 6. From the measured branching fractions for $\psi K^{(*)}$, we expect $a_2/a_1 \simeq 0.22$. Using the QCD Wilson coefficients $c_1(m_b^2) = 1.12$ and $c_2(m_b^2) = -0.26$, and $1/N_c$ 1/3, we expect $a_1 = 1.03$ and $a_2/a_1 = 0.11$. This is, at least, "in the ballpark", suggesting that factorization and perturbative-QCD work at some level in describing these decays.

The Class II (color-suppressed) decays of the form $B^0 \to D^{(*)0}$ plus one neutral meson have been searched for. No signal has been seen in any mode, and 90% CL upper limits have been set (Table 2). All limits are above, but some are approaching, theoretical expectations [4, 5]. The limits are 5–15% of analogous charged final state. This is to be contrasted with the pattern in D decays; for example: $\mathcal{B}(D^0 \to K^0\pi^0)/\mathcal{B}(D^0 \to K^-\pi^+) = 0.57 \pm 0.13$. Color suppression is clearly operable in B decays. The only color-suppressed decays that have been seen so far are the $\psi K^{(*)}$ final states, which have branching fractions at the 10^{-4} level.

2.2 Test of Factorization

In the factorization approximation, the rate for a Class I decay such as $\overline{B}^0 \to D^{*+}h^-$ can be related to the differential rate for $\overline{B}^0 \to D^{*+}\ell^-\overline{\nu}_\ell$ at the appropriate $q^2 \equiv m^2(\ell\overline{\nu}_\ell)$ (for which factorization is exact). The relation is:

$$\frac{\mathcal{B}(\overline{B}^0 \to D^{*+}h^-)}{\frac{d\mathcal{B}}{dq^2}(\overline{B}^0 \to D^{*+}\ell^-\overline{\nu}_\ell)|_{q^2=m_h^2}} = 6\pi^2 a_1^2 f_h^2 |V_{ud}|^2$$

We take the branching fractions reported above for the cases $h^- = \pi^-$, ρ^-, a_1^-, and use theoretical models to extrapolate the measured $\frac{d\mathcal{B}}{dq^2}$ to $q^2 = m_h^2$, in order to evaluate the left hand side of the above equation (R_{exp}) and compare in Table 4 with the theoretical prediction for the right hand side (R_{theo}).

We see good agreement within errors, but only the low q^2 region of the $B \to D^{(*)}X$ decay is being probed in these tests. One can also compare the observed polarization of the D^* in $\overline{B}^0 \to D^{*+}\rho^-$ decays to that in $\overline{B}^0 \to D^{*+}\ell^-\nu_\ell$; one again finds consistency [6] with the expectation from factorization.

Some conclusions: Our catalog of quasi- two-body hadronic B decays covers $< 12\%$ of all the total hadronic B decay rate. For these low-multiplicity decays, the interference between the external and internal W emission diagrams (in Class III decays) is constructive. The models are in qualitative agreement with the data. Color suppression appears to be active in B decays. Factorization appears to be valid for low$-q^2$ hadronic decays that proceed via external W emission.

3 Rare B Decays

In the last few years, CLEO has discovered several classes of rare decays (*i.e.*, decays that do not proceed via $b \to cW$):

- 1993: First observation of unambiguous penguin decays: $B \to K^*\gamma$ [7].
- 1994: Observation of inclusive $b \to s\gamma$ (at $\sim$ SM level) [8].
- 1995: charmless hadronic decay: h^+h^- (mixture of $\pi^+\pi^-$ from $b \to u\bar{u}d$ and $K^+\pi^-$ from $b \to sg$) [9].
- 1996: Exclusive $b \to u\ell\nu$ ($\pi\ell\nu$, $\rho\ell\nu$) [10], and significant $K^+\pi^-$ signal.
- 1997: MANY more modes discovered: $K_s^0\pi^+$, $K^+\pi^0$, ωK^+, ωK_s^0, ϕK^*, $\eta' K^+$, $\eta' K_s^0$, η' inclusive [11, 12, 13].

In a typical rare decay search analysis, we aim for branching fraction sensitivity at the (few)$\times 10^{-5}$ level and efficiencies in the 2$-$25% range, depending on mode. The typical background level is of the same order as signal. In modes for which charged π/K separation is important, this ability is the main contribution to the systematic error of the measurement.

Experimental variables which distinguish signal from background include those mentioned in the introduction (ΔE, M_b, event shape, dE/dx for π/K separation), as well as more detailed measures: the event energy flow around the decay candidate, quantified using a Fisher Discriminant technique; the angle between the candidate thrust axis and the beam axis; and the angle between the candidate flight direction and the beam axis.

In the simple "cut-and-count" analysis, we cut on these variables, and produce histograms in ΔE versus M_b space (or their projections) to extract the signal. However, these variables provide signal/ background separation on a statistical basis; so in an optimized analysis, they are used as inputs to a multi-dimensional likelihood fit to extract the signal and background contributions, and sort out the charged π/K content of the mode. The results are presented as histograms in M_b or ΔE from the cut-and-count analysis, along with smooth curves from the likelihood fit. The measured branching fraction and its significance, or the upper limit, is extracted from the likelihood fit.

3.1 $\bar{B}^0 \to \pi^-\pi^+$, $K^-\pi^+$, K^-K^+

The $\pi^-\pi^+$ final state is expected to proceed via a $b \to u\bar{u}d$ tree diagram, with the $b \to d\bar{u}u$ penguin sub-dominant (see Fig. 1). The $K^-\pi^+$ final state is expected to proceed via a $b \to s\bar{u}u$ penguin diagram, with the $b \to u\bar{u}s$ tree sub-dominant. The K^-K^+ final state is dynamically suppressed; it could arise, for example, through a $b \to d\bar{s}s$ penguin followed by charge-exchange rescattering.

Previously, CLEO was unable to establish significant signals in $\pi^-\pi^+$ or $K^-\pi^+$ separately, although there was a $> 3\sigma$ signal in the sum of the two modes [9]. Since 1995, 30% more data was added, and the analysis was re-optimized. CLEO now reports a significant signal in the $K^-\pi^+$ final state (5.6σ; see Fig. 2(a)), and no significant signal in $\pi^-\pi^+$. In addition, there is a significant signal in the $h^-K^0_S$ final state (Fig. 2(b)), and the hint of one in the and $h^-\pi^0$ final state, where h^- represents either a π^- or a K^-. The branching fractions for the significant signals are given in Table 5.

3.2 Modes with ρ, K^*, ϕ, ω, η, η'

These are a broad class of low-multiplicity B decay modes which proceed via $b \to u$ and/or $b \to s$, which are potentially useful modes for measuring the CKM angle γ, and/or for understanding penguin amplitudes. Here, the resonance mass, and the decay angles and/or Dalitz plot densities, provide extra handles to enhance signal over background, allowing the event shape cuts to be loosened.

Statistically significant signals have been seen (Fig. 3), and their branching fractions summarized in Table 5, in the following final states: $B^+ \to \omega K^+$ and $\omega\pi^+$, $B^+ \to \eta' K^+$, $B^0 \to \eta' K^0$, and $B^+ \to \phi K^{*+}$. In addition, there is a significant signal for inclusive η' production [14], consistent with $\eta' X_s$, where X_s is a low-mass $Kn\pi$ system.

No signal has been seen, and upper limits have been set [11, 12, 13], on various charge combinations of: $\pi\pi$, $\pi\rho$, $K\rho$, $K^*\pi$, KK, KK^*, $K\phi$, $\omega\rho$, ωK^*, $\eta\pi$, $\eta\rho$, ηK, ηK^*, $\eta'\pi$, $\eta'\rho$, $\eta' K^*$.

3.3 Why is B($B^+ \to \eta' K^+$) so large?

It is interesting to note that significant signals are emerging in modes containing η', but not yet η (despite the greater experimental sensitivity). It was expected [15] that the ratio $\mathcal{B}(\eta' K^-)/\mathcal{B}(\eta K^-)$ would be large due to interference between the $b \to s\bar{s}s$ and $b \to s\bar{u}u$ penguin diagrams, both of which contribute to both final states. There may also be enhancements due to other, less well understood effects [16] such as (a) the OZI suppressed "hairpin" process $b \to s\eta, \eta'$; (b) $b \to c\bar{c}s$ with a large $c\bar{c}$ component in the η' wavefunction; (c) final state rescattering from $\eta_c K \to \eta' K$; (d) an anomalous $gg\eta'$ coupling.

3.4 Search for Inclusive $b \to s\ell^+\ell^-$

In the Standard Model, several processes contribute to $b \to s\ell^+\ell^-$, including penguin and box diagrams (Fig. 4). The process does not have large QCD corrections and thus can be used to constrain new physics which might appear in the loops, such as SUSY, charged Higgs bosons, and new neutral bosons [18].

CLEO does a "quasi-inclusive" search [17] similar to the one performed in the observation of $b \to s\gamma$ [8]. One reconstructs the final state $K(n\pi)\ell^+\ell^-$, where the pions may be charged or neutral, $n = 0...4$, but at most one π^0 is allowed. The K may be charged (identified via dE/dx and TOF) or $K^0_S \to \pi^+\pi^-$. The only significant background is from $K^{(*)}\psi^{(\prime)}$, so the $m(\ell^+\ell^-)$ region near ψ and ψ' are excluded. No signal is seen; the branching fraction upper limits are given in Table 6 along with the Standard Model predictions. The limits are significantly better than previous ones (the UA1 limit [19] was for $M(\mu^+\mu^-) > 3.9$ GeV only), but they are still a factor ~ 10 above the SM prediction.

4 Semileptonic B Decay

CLEO has previously published papers [20] on the semileptonic decay $B \to D^*\ell\overline{\nu}$, focussing on the branching fraction, the extraction of V_{cb}, and the measurement of the form factors in the decay. This summer, there are new (or updated) results on $B \to D\ell\overline{\nu}$, $D_J\ell\overline{\nu}$ (where D_J are the P-wave D mesons), and the pure $b \to u$ process $\rho\ell^-\overline{\nu}_\ell$. These semileptonic decays are all more difficult to isolate than $D^*\ell\overline{\nu}$, since the former has the largest branching fraction of all exclusive semileptonic decays, and because the narrow width of the D^* makes it easy to isolate from non-D^* backgrounds.

In all cases, however, CLEO has excellent lepton identification. The hermiticity of the detector can be used to identify neutrinos, aiding in background reduction at some cost in efficiency.

4.1 $B \to D\ell\overline{\nu}$

In this mode, the ℓ ($e^\pm$ or $\mu^\pm$) and D ($D^0 \to K^-\pi^+$ or $D^+ \to K^-\pi^+\pi^+$) are explicitly reconstructed. The hermiticity of the detector is used to reconstruct the neutrino, which is necessary in order to suppress the large background from $D^*\ell\nu$. It also improves the resolution on $q^2 = m^2(\ell\nu)$, in order to measure the $B \to D$ form factor. The branching fraction, and the differential rate $d\Gamma/dq^2$, is extracted from fits to the beam-constrained mass distribution in the data (Fig. 5), using Monte Carlo predictions for the signal and for the (of order 50%) backgrounds from $D^{**}\ell\overline{\nu}$, $D^*\ell\overline{\nu}$, combinatoric (D and ℓ from different B's), fake leptons, and continuum.

The $D^0\ell\overline{\nu}$ and $D^+\ell\overline{\nu}$ are combined for the study of the differential rate. The data are analyzed in terms of q^2 or the Heavy Quark Effective Theory (HQET) variable $w \equiv v_B \cdot v_D = (M_B^2 + M_D^2 - q^2)/(2M_BM_D)$; and the form factor is defined as follows:

$$\begin{aligned}
\frac{d\Gamma}{dw} &= \frac{1}{4N_{\Upsilon(4S)}}\left[\frac{N_0(w)}{\tau_{B^-}\mathcal{B}_{D^0}\epsilon_0(w)} + \frac{N_+(w)}{\tau_{B^0}\mathcal{B}_{D^+}\epsilon_+(w)}\right] \\
&= \frac{G_F|V_{cb}|^2}{48\pi^3}(m_B+m_D)^2(m_D\sqrt{w-1})^3\mathcal{F}_D(w)^2 \\
\mathcal{F}_D(w) &= \mathcal{F}_D(1)\left(1-\rho_D^2(w-1)+c_D(w-1)^2\right)
\end{aligned}$$

The results of the fits to the data [24] are (Fig. 6):

$$\begin{aligned}
\mathcal{F}_D(1)|V_{cb}| &= (3.37 \pm 0.44 \pm 0.48^{+0.53}_{-0.12}) \times 10^{-2} \\
\rho_D^2 &= 0.59 \pm 0.22 \pm 0.12^{+0.59}_{-0} \\
\Gamma(\overline{B} \to D\ell\overline{\nu}) &= (12.0 \pm 0.9 \pm 2.1)ns^{-1} \\
\mathcal{B}(\overline{B}^0 \to D^+\ell^-\overline{\nu}) &= (1.87 \pm 0.15 \pm 0.32)\% \\
\mathcal{B}(\overline{B}^- \to D^0\ell^-\overline{\nu}) &= (1.94 \pm 0.15 \pm 0.34)\%
\end{aligned}$$

Taking $\mathcal{F}_D(1) = 0.98 \pm 0.07$ [21] we find $|V_{cb}| = (3.44 \pm 0.45 \pm 0.49^{+0.54}_{-0.12} \pm 0.25) \times 10^{-2}$, consistent with other measurements ($D^*\ell\overline{\nu}$, $X\ell\overline{\nu}$).

The form factor has also been measured by CLEO in the $D^*\ell\overline{\nu}$ decay [20], and we find:

$$\mathcal{F}_D(1)/\mathcal{F}_{D^*}(1) = 0.96 \pm 0.20, \quad \text{and} \quad \rho^2_D - \rho^2_{D^*} = -0.25 \pm 0.29.$$

This confirms the HQET prediction of similar normalizations and slopes for the two decay modes.

4.2 $B \to D_J\ell\overline{\nu}$

Some 60–70% of the $B \to X\ell\overline{\nu}$ inclusive rate is from $D\ell\overline{\nu}$ and $D^*\ell\overline{\nu}$ [25]; the remainder is expected to be mainly from $D_J\ell\overline{\nu}$ (narrow P-wave), $D_J\ell\overline{\nu}$ (broad P-wave), and $D^{(*)}\pi\ell\nu$ non-resonant ($b \to u\ell\overline{\nu}$ is small). Models (*e.g.*, ISGW2 [22]) predict $D_J\ell\overline{\nu}$ to be small. There are few reliable models for the $D^{(*)}\pi\ell\nu$ non-resonant component; they tend to predict a very small rate [23]. It is unclear from these predictions whether the $D_J\ell\overline{\nu}$ and non-resonant decay rates are sufficient to saturate the total inclusive semileptonic decay rate. It is thus important to measure these rates accurately.

The $D_J\ell\overline{\nu}$ (broad P-wave) and $D^{(*)}\pi\ell\nu$ non-resonant decays suffer from large combinatoric background at CLEO. We thus concentrate on isolating signals for the narrow P-wave $D_J\ell\overline{\nu}$ decays by fully reconstructing the $D_J\ell$ system. The decay chain used is: $B^- \to D^0_J\ell^-\overline{\nu}$, $D^0_J \to D^{*+}\pi^-$, $D^{*+} \to D^0\pi^+_s$, and $D^0 \to K^-\pi^+$. To suppress the large combinatoric background from $D^{*+}\ell^-\overline{\nu}$ with a pion from the other B, we require kinematic inconsistency with $D^{*+}\ell^-\overline{\nu}$. We then fit $\delta M_J \equiv M(D^{*+}\pi^-) - M(D^{*+})$ in the data with narrow Breit Wigner lineshapes for $D^0_1(2420)$ and $D^{*0}_2(2460)$.

The results of the fit [26] are shown in Figure 7 and Table 7, where we have assumed the branching fractions $\mathcal{B}(D^0_1 \to D^{*+}\pi^-) = 67\%$ and $\mathcal{B}(D^{*0}_2 \to D^{*+}\pi^-) = 20\%$. They are consistent with the model predictions, leaving room for 15–20% of the $B \to X\ell\overline{\nu}$ inclusive rate from $D_J\ell\overline{\nu}$ (broad P-wave), $D^{(*)}\pi\ell\nu$ non-resonant decays.

4.3 $b \to u\ell^-\overline{\nu}_\ell$

Because the $b \to u\ell^-\overline{\nu}_\ell$ process has a very small branching fraction, large backgrounds, and missing energy from the neutrino, we focus on the measurement of exclusive final states $\pi^-\ell^+\nu$, $\rho^-\ell^+\nu$, and $\omega\ell^+\nu$. A measurement of the branching fractions to these modes requires models for kinematical distributions (shapes of form factors); the extraction of $|V_{ub}|$ from the branching fractions requires absolute normalization of the form factors as well. These can be obtained from quark models, lattice QCD, and QCD sum rules.

In 1996, CLEO used events containing leptons with momentum above 1.5 GeV/c, and measured [10] $\mathcal{B}(B^0 \to \rho^- \ell^+ \nu) = (2.5 \pm 0.4^{+0.3}_{-0.4} \pm 0.5) \times 10^{-4}$ and $\mathcal{B}(B^0 \to \pi^- \ell^+ \nu) = (1.8 \pm 0.4 \pm 0.3 \pm 0.2) \times 10^{-4}$. From these, we extracted $|V_{ub}| = (3.3 \pm 0.2^{+0.3}_{-0.4} \pm 0.7) \times 10^{-3}$, where the last error is due to model dependence.

That analysis suffered from considerable background, especially at low lepton momentum. This summer, we report preliminary results [27] from a new analysis that focuses on leptons with momentum above 2.3 GeV/c, which is above $b \to c\ell\nu$ endpoint. Many other cuts were loosened, and $\sim 30\%$ more luminosity was added; thus, the new analysis is largely statistically independent of the 1996 result.

The final states $\rho^- \ell^+ \nu$, $\rho^0 \ell^+ \nu$, and $\omega \ell^+ \nu$ were reconstructed, using detector hermiticity to require the event to be consistent with containing exactly one neutrino. To extract the branching fractions, all the modes were combined by constraining the relative decay rates to predictions from isospin and the quark model:

$$\Gamma(B^0 \to \rho^- \ell^+ \nu) = 2 \times \Gamma(B^+ \to \rho^0 \ell^+ \nu) = 2 \times \Gamma(B^+ \to \omega \ell^+ \nu).$$

The result is shown in Figure 8. A fit using several different kinematical variables is used to extract the signal from backgrounds and cross-feeds from other $b \to u\ell\nu$ final states. The (very) preliminary branching fraction, within the ISGW2 model, is $\mathcal{B}(B^0 \to \rho^- \ell^+ \nu) = (2.0 \pm 0.3 \pm 0.3) \times 10^{-4}$. The result is consistent with the 1996 CLEO result. No model dependence has been evaluated yet, so it is premature to combine these results with those of the previous analysis.

5 Summary

In this talk, I have covered only three categories of recent results from CLEO on B decays. For further information, refer to Ref. [28].

- With large sample of fully-reconstructed $b \to c$ hadronic decays, we are probing models, observing color suppression, and testing factorization.

- We are now observing several classes of rare charmless decays, probing $b \to u$ and $b \to s$ transitions. These provide handles on the CKM matrix elements V_{bu}, V_{ts}, and V_{td}, and ultimately may give evidence for CP violation in B decays.

- The detailed study of exclusive semileptonic decays test Heavy Quark Effective Theory and form factor models, and permit the extraction of $|V_{ub}|$. Further progress requires better measurements and a deeper understanding of non-resonant $D^{(*)}(n\pi)\ell\overline{\nu}_\ell$ decay rates.

6 Future

The CLEO III detector[29] is scheduled to begin data taking in 1999, when the upgraded CESR collider will be delivering instantaneous luminosities in the range $1-3\times 10^{33}$ cm^{-2} s^{-1}. CLEO III will feature an entirely new inner detector: new silicon vertex detector, drift chamber, fast RICH for K/π separation at momenta up to 2.6 GeV, a new data acquisition system, and new software infrastructure. Many of the difficulties that CLEO II experiences in the study of rare B decays with limited K/π separation will disappear when the CLEO III RICH is used. In addition, improved charged particle tracking and momentum resolution will enhance our ability to kinematically separate strange- and non-strange final states. A data set of $30-50$ fb^{-1} will allow us to make precision measurements that will severely challenge the Standard Model and take our understanding of B physics to the next level, including the reconstruction of exclusive $b\to u$ final states and a full analysis of many exclusive $b\to s$ decays.

High on the list of physics topics that CLEO III will explore is the study of $B\to\pi^+\pi^-$ and $K^+\pi^-$. These measurements are crucial to our understanding of $|V_{ub}|$, tree diagram amplitudes, and $b\to sg$ penguin amplitudes. Both of these decay modes are candidates for the observation of CP violation. Since CP violation in $\pi^+\pi^-$ involves mixing, it is best studied at an asymmetric B factory. Extracting the CP violating angle α from the time-dependent CP asymmetries in this mode may also require precision measurements of the time-integrated rates for $\pi^+\pi^0$ and $\pi^0\pi^0$ [30], which will require high luminosity. The $K^+\pi^-$ mode is self-tagging and the observation of CP violation does not require a lifetime-dependent measurement; but it does require a non-zero strong interaction phase shift. This mode is sensitive to the CP violating angle γ, as well as to any CP violating phases in the $b \to sg$ penguin process. Another set of modes which are sensitive to γ and which are within reach of CLEO III is $B \to DK^{(*)}$. It will also be possible to study many $b \to sg$ decay modes of the form $K^{(*)}$ plus π, ρ, ω, or ϕ in various charge combinations. Measurements of $B \to \rho\gamma$ along with $B \to K^*\gamma$ will provide information on V_{ts}/V_{td}. Tests of factorization and HQET will evolve into studies of violations of these predictions. Many other topics in rare B physics will come within reach.

However, some important measurements will remain out of reach of even CLEO III and the asymmetric B factories. Although CP violation in $B \to K\pi$ and $DK^{(*)}$ may be observed by CLEO III, it will not be possible to extract the value of the CKM angle γ without knowing the magnitude of the interfering tree and penguin amplitudes. These can be determined by measuring time-integrated rates for a whole family of related decays (some heavily suppressed) [30], which requires much more luminosity than will be available in the B factory era. Also, the accurate measurement of $b \to s\ell^+\ell^-$ inclusive and exclusive decays at the Standard Model level, and the leptonic decays $B \to \mu\nu$ and $\tau\nu$, will likely require several hundred million $B\bar{B}$ events. In order to achieve such large data samples, the CESR and CLEO groups have begun to explore plans for another upgrade (referred to as "Phase IV") of the collider (this time, involving two rings embedded in dual-aperture magnets) and the detector. Working groups within CLEO have been studying the physics justification and the minimal requirements for a detector operating at luminosities capable of delivering 200-600 million $B\bar{B}$ events in a 3 year run. Planning for such an experiment is only now beginning.

Acknowledgements

The CLEO Collaboration gratefully acknowledges the effort of the CESR staff in providing excellent luminosity and running conditions. This work was supported by the NSF, the DoE, and the NSERC of Canada. Finally, the author thanks the organizers of Beauty '97 for a most stimulating series of talks.

References

[1] CLEO Collaboration, *Exclusive Reconstruction of $B \to D^{(*)}(n\pi)^-$ Decays*, CLEO-CONF 97-01 (1997).

[2] CLEO Collaboration, *Search for Color-Suppressed B Hadronic Decay Processes with CLEO*, CLEO-CONF 97-12 (1997).

[3] M. Bauer, B. Stech, and M. Wirbel, Z. Phys. C 29, 637 (1985); *ibid* 34, 103 (1987); *ibid* 42, 671 (1989).

[4] M. Neubert, V. Rieckert, B. Stech and Q.P. Xu in *Heavy Flavours*, edited by A.J. Buras and H. Lindner, World Scientific, Singapore (1992).

[5] A. Deandrea, N. Di Bartolomeo, R. Gatto and G. Nardulli, Phys. Lett. B 318, 549 (1993).

[6] T.E. Browder and K. Honscheid, Prog. Part. Nucl. Phys. 35, 81 (1995).

[7] R. Ammar *et al.* (CLEO Collaboration), Phys. Rev. Lett. 71, 674 (1993).

[8] M.S. Alam *et al.* (CLEO Collaboration), Phys. Rev. Lett. 74, 2885 (1995).

[9] D.M. Asner *et al.* (CLEO Collaboration), Phys. Rev. D53, 1039 (1996).

[10] J.P. Alexander *et al.* (CLEO Collaboration), Phys. Rev. Lett. 77, 5000 (1996).

[11] CLEO Collaboration, *Observation of Exclusive Rare Charmless B Decays*, CLEO-CONF 97-24 (1997).

[12] CLEO Collaboration, *Search for Charmless Hadronic Decays of B Mesons to Final States Including ω or ϕ Mesons*, CLEO-CONF 97-23 (1997).

[13] CLEO Collaboration, *Study of Charmless Hadronic Decays of B Mesons With Final States Including η or η' Mesons*, CLEO-CONF 97-22A (1997).

[14] CLEO Collaboration, *Observation of Inclusive $B \to \eta' X_s$ Decays*, CLEO-CONF 97-13 (1997).

[15] H.J. Lipkin, Phys. Lett. B 254, 247 (1991).

[16] See citations in Ref. [13].

[17] CLEO Collaboration, *Searching For Inclusive* $b \to s\ell^+\ell^-$, CLEO-CONF 97-15 (1997).

[18] See citations in Ref. [17].

[19] Albajar *et al.* (UA1 Collaboration), Phys. Lett. B 262, 163 (1991).

[20] B. Barish *et al.* (CLEO Collaboration), Phys. Rev. D 51, 1014 (1995); J.E. Duboscq *et al.* (CLEO Collaboration), Phys. Rev. Lett 76, 3898 (1996).

[21] I. Caprini and M. Neubert, Phys. Lett. B 380, 376 (1996).

[22] D. Scora and N. Isgur, Phys. Rev. D 52, 2783 (1995).

[23] J.L. Goity and W. Roberts, Phys. Rev. D 51, 3459 (1995).

[24] CLEO Collaboration, *Measurement of the* $B \to D\ell\nu$ *Partial Width and Form Factor Parameters*, CLEO-CONF 97-02 (1997).

[25] See, for example, J.D. Richman and P.R. Burchat, Rev. Mod. Phys. 67, 893 (1995).

[26] CLEO Collaboration, *Evidence of* D_J *production in semileptonic B decay* , CLEO-CONF 97-21 (1997).

[27] CLEO Collaboration, *A New Measurement of the* $b \to u$ *Semileptonic Decays* $B \to \rho\ell\nu$ *and* $B \to \omega\ell\nu$, CLEO-CONF 97-30 (1997).

[28] `http://www.lns.cornell.edu/public/CLNS/CLEO.html` and `http://www.lns.cornell.edu/public/CONF/`.

[29] A. Wolf, these Proceedings.

[30] I. Dunietz, these Proceedings.

Table 1: Yields and branching fractions for color-allowed decays of the form $D^{(*)}(n\pi)^-$.

B Mode	yield	$\mathcal{B}(\%)$
$D^+\pi^-$	240	$(0.250 \pm 0.022 \pm 0.024 \pm 0.024)$
$D^{*+}\pi^-$	248	$(0.234 \pm 0.021 \pm 0.022 \pm 0.010)$
$D^0\pi^-$	1014	$(0.473 \pm 0.025 \pm 0.033 \pm 0.014)$
$D^{*0}\pi^-$	207	$(0.392 \pm 0.046 \pm 0.033 \pm 0.028)$
$D^+\rho^-$	251	$(0.789 \pm 0.069 \pm 0.093 \pm 0.077)$
$D^{*+}\rho^-$	250	$(0.734 \pm 0.061 \pm 0.074 \pm 0.030)$
$D^0\rho^-$	744	$(0.920 \pm 0.080 \pm 0.072 \pm 0.028)$
$D^{*0}\rho^-$	217	$(1.277 \pm 0.129 \pm 0.113 \pm 0.090)$
$D^+a_1^-$	136	$(0.834 \pm 0.088 \pm 0.115 \pm 0.081)$
$D^{*+}a_1^-$	160	$(1.157 \pm 0.120 \pm 0.155 \pm 0.049)$
$D^0a_1^-$	242	$(0.887 \pm 0.104 \pm 0.107 \pm 0.028)$
$D^{*0}a_1^-$	109	$(1.597 \pm 0.250 \pm 0.209 \pm 0.115)$

Table 2: Yields and branching fractions for color-suppressed decays of the form $D^{(*)0}(n\pi)^0$.

B Mode	$\mathcal{B}(\times 10^{-4})$	B Mode	$\mathcal{B}(\times 10^{-4})$
$B^0 \to D^0\pi^0$	< 1.2	$B^0 \to D^{*0}\pi^0$	< 4.4
$B^0 \to D^0\rho^0$	< 3.9	$B^0 \to D^{*0}\rho^0$	< 5.6
$B^0 \to D^0\eta$	< 1.3	$B^0 \to D^{*0}\eta$	< 2.6
$B^0 \to D^0\eta'$	< 9.4	$B^0 \to D^{*0}\eta'$	< 19
$B^0 \to D^0\omega$	< 5.1	$B^0 \to D^{*0}\omega$	< 7.4

Table 3: Results of fit to BSW parameters.

Model	$\|a_1\|$
CDDFGN	$0.953 \pm 0.026 \pm 0.042 \pm 0.020$
BSW	$0.989 \pm 0.028 \pm 0.043 \pm 0.021$
Model	a_2/a_1
CDDFGN	$0.232 \pm 0.037 \pm 0.022 \pm 0.018$
BSW	$0.264 \pm 0.039 \pm 0.025 \pm 0.019$

Table 4: Tests of factorization using $\overline{B}^0 \to D^{*+}h^-$ decays.

q^2	R_{exp} (GeV^2)	R_{theo} (GeV^2)
m_π^2	$1.3 \pm 0.1 \pm 0.2$	1.2 ± 0.2
m_ρ^2	$3.4 \pm 0.3 \pm 0.5$	3.3 ± 0.5
$m_{a_1}^2$	$3.8 \pm 0.4 \pm 0.5$	3.0 ± 0.5

Table 5: Branching fractions for rare B decays with significant signals.

Mode	Branching fraction
ωK	$(1.5^{+0.7}_{-0.6} \pm 0.3) \times 10^{-5}$
$\omega\pi$	$(1.1^{+0.6}_{-0.5} \pm 0.2) \times 10^{-5}$
$\eta' K$	$(7.1^{+2.5}_{-2.1} \pm 0.9) \times 10^{-5}$
$\eta' K^0$	$(5.3^{+2.8}_{-2.2} \pm 1.2) \times 10^{-5}$
ϕK^*	$(1.3^{+0.7}_{-0.6} \pm 0.2) \times 10^{-5}$
$K^+\pi^-$	$(1.5^{+0.5}_{-0.4} \pm 0.1) \times 10^{-5}$
$K^0\pi^+$	$(2.3^{+1.1}_{-1.0} \pm 0.2) \times 10^{-5}$
$\eta' X_s$	$(62 \pm 16 \pm 13) \times 10^{-5}$

Table 6: Upper limits on branching fractions for $b \to s\ell^+\ell^-$ decays.

mode	90% CL limit	SM (Ali)
se^+e^-	5.7×10^{-5}	$(0.8 \pm 0.2) \times 10^{-5}$
$s\mu^+\mu^-$	5.6×10^{-5}	$(0.6 \pm 0.1) \times 10^{-5}$
$se^\pm\mu^\mp$	2.2×10^{-5}	0

Table 7: Results of fit for $B^- \to D_J^0 \ell^- \overline{\nu}$ events.

D_J	Yield	$\mathcal{B}(B^- \to D_J^0 \ell^- \overline{\nu})$
$D_1^0(2420)$	53.5 ± 12.2	$(0.56 \pm 0.13 \pm 0.08 \pm 0.04)\%$
$D_2^{*0}(2460)$	8.8 ± 9.8	$< 0.8\%$ (90% CL)

FIGURE CAPTIONS

Figure 1: Feynman diagrams for the decays $\bar{B}^0 \to K^- \pi^+$. Left: tree diagram; right: penguin diagram.

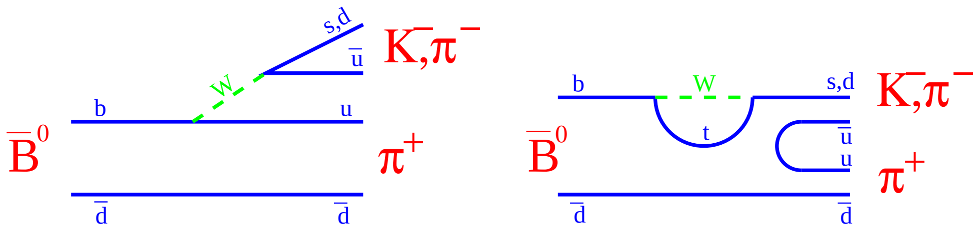

Figure 2: The beam-constrained mass for the $B^0 \to K^+\pi^-$ (left) and $B^+ \to K^0_S K/\pi^+$ (right) searches. The histogram is the result of the "cut-and-count" analysis; the curve is the result of the likelihood fit.

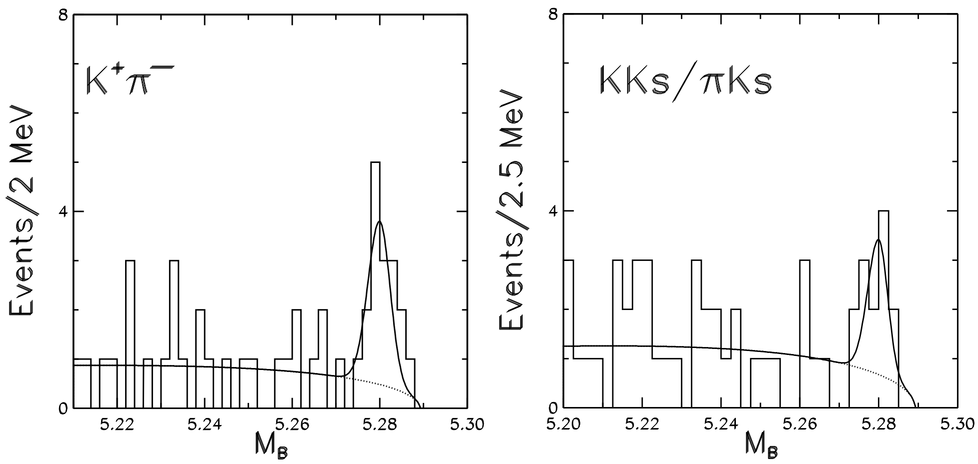

Figure 3: The beam-constrained mass for (a) $B^+ \to \eta' h^+$; (b) $B^0 \to \eta' K_S^0$; (c) $B^+ \to \omega h^+$, where h^+ is a pion or a kaon. The histogram is from the cut-and-count analysis; the curve is from the likelihood fit.

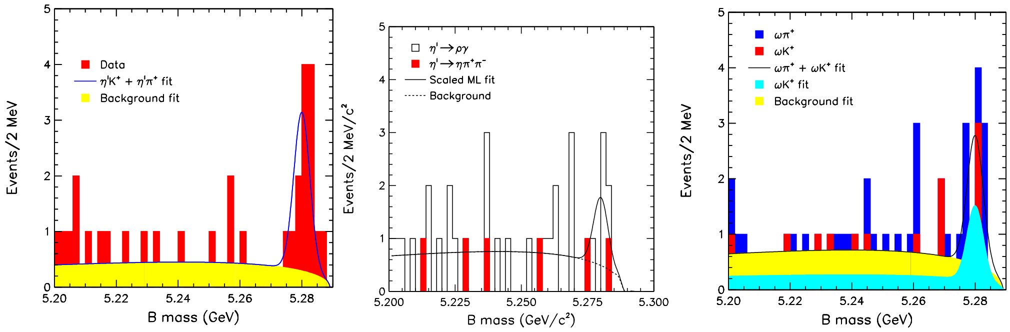

Figure 4: Feynman diagrams for the quark-level decays $b \to s\ell^+\ell^-$. Left: penguin diagram; right: box diagram.

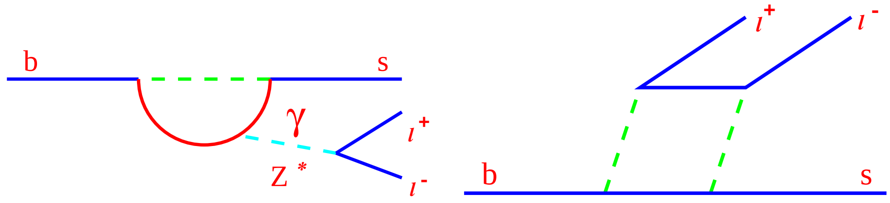

Figure 5: Beam-constrained mass distributions for the $D^0\ell^-\overline{\nu}$ (top) and $D^+\ell^-\overline{\nu}$ (bottom) decays. The points are data. $D\ell\overline{\nu}$ events. Points: data. Histograms (from top to bottom): Monte Carlo predictions for signal (open histogram), $D^{**}\ell\overline{\nu}$, $D^*\ell\overline{\nu}$, combinatoric background, fake leptons/continuum.

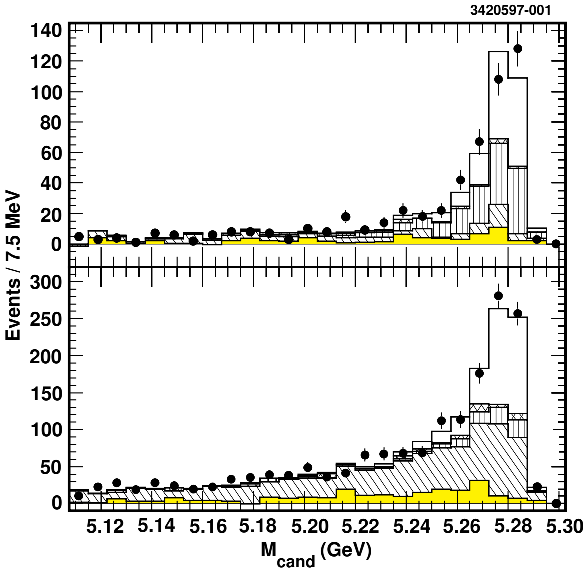

Figure 6: (a) $d\Gamma/dw$ distribution from the data (points), and result of the fit with a linear slope (histogram). (b) Measured values of $\mathcal{F}_D(w)|V_{cb}|$ (points), the fit results with statistical errors (solid and dashed lines), and the function $\mathcal{F}_{D^*}(w)|V_{cb}|$ obtained from an analysis of $\bar{B} \to D^*\ell\overline{\nu}$ decays (dotted line).

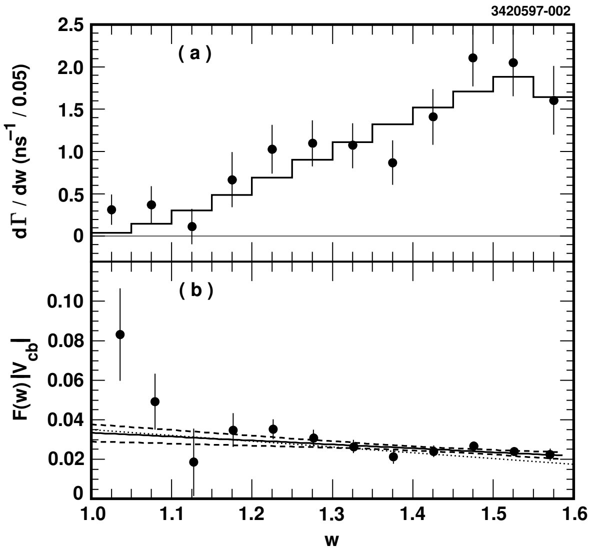

Figure 7: The δM_J distribution for $B^- \rightarrow D_J^0 \ell^- \overline{\nu}$ candidates in the data (points), and a fit to the $D_1^0(2420)$ and $D_2^{*0}(2460)$ resonances over a smooth background (curve).

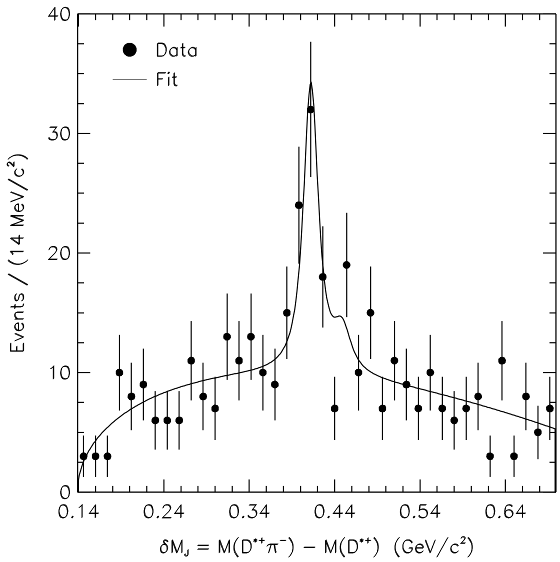

Figure 8: $M(\pi\pi)$ distribution for $B \to \rho\ell\overline{\nu}$ candidate events with high momentum leptons (> 2.3 GeV/c). The points are data after continuum subtraction. The histograms (top to bottom) show the estimated contributions from correctly-identified $B \to \rho\ell\overline{\nu}$ (open histogram), cross-feed from $B \to \rho\ell\overline{\nu}$ and $\omega\ell\overline{\nu}$; other $b \to u\ell\overline{\nu}$, and $b \to c\ell\overline{\nu}$.